
Article:
Rennie, A.J.R., Martins, V.L., Torresi, R.M et al. (1 more author) (2015) Ionic Liquids Containing Sulfonium Cations as Electrolytes for Electrochemical Double Layer Capacitors. The Journal of Physical Chemistry C, 119 (42). pp. 23865-23874. ISSN 1932-7447

https://doi.org/10.1021/acs.jpcc.5b08241

THE JOURNAL OF PHYSICAL CHEMISTRY C

Article

Ionic Liquids Containing Sulfonium Cations as Electrolytes for Electrochemical Double Layer Capacitors

Anthony J. R. Rennie, Vitor L Martins, Roberto Manuel Torresi, and Peter Joseph Hall

J. Phys. Chem. C, **Just Accepted Manuscript** • DOI: 10.1021/acs.jpcc.5b08241 • Publication Date (Web): 30 Sep 2015

ACS Publications

The Journal of Physical Chemistry C is published by the American Chemical Society. 1155 Sixteenth Street N.W., Washington, DC 20036

Ionic Liquids Containing Sulfonium Cations as Electrolytes for Electrochemical Double Layer Capacitors

Anthony J. R. Rennie,[*,a,‡] *Vitor L. Martins,*[a,b,‡] *Roberto M. Torresi,*[b] *and Peter J. Hall*[*,a]

AUTHOR ADDRESS

[a] Chemical and Biological Engineering, University of Sheffield, Sir Robert Hadfield Building, Mappin Street, Sheffield S1 3JD, England, UK

[b] Instituto de Química, Universidade de São Paulo - C.P. 26077, CEP 05513-970, São Paulo, SP, Brazil

ABSTRACT

In this work we report on the behavior of ionic liquids (ILs) containing sulfonium cations as electrolytes for electrochemical double layer capacitors (EDLCs). Physical properties such as viscosity and ionic conductivity are reported over a range of temperatures for ILs containing the diethylmethyl sulfonium [S_{221}], triethyl sulfonium [S_{222}] and dimethylpropyl sulfonium [S_{223}] cations paired with the bis(trifluoromethanesulfonyl) imide [Tf_2N] anion. The size and structure of the cations are shown to influence the physical and electrochemical properties of the ILs, with

a significant degree of ionic coordination being evident in $[S_{223}][Tf_2N]$. The electrochemical behavior of these ILs in EDLCs was compared with that of a fairly established IL electrolyte, *N*-butyl-*N*-methylpyrrolidinium bis(trifluoromethanesulfonyl) imide ($[Pyr_{14}][Tf_2N]$), and it is shown that $[S_{221}][Tf_2N]$ can perform better in terms of energy and power at room temperature, despite operating at a much reduced potential.

Introduction

Electrochemical double-layer capacitors (EDLCs) are a class of energy storage device known for their high power densities (up to 10kW kg^{-1}).[1–3] Their ability to accept or deliver charge at substantially higher rates than electrochemical cells suitable for use in applications where peak demand is substantially greater than the average load.[4,5] Other desirable features of EDLCs are that they possess long cycle live (in excess of 500,000 cycles) and relatively high energy efficiencies.[1–7] Consequently, EDLCs can be used to produce systems that require less maintenance than those where energy is stored in batteries.

Conventional EDLCs are comprised of activated carbon based electrodes, an electrically insulating separator and an organic electrolyte solution.[1–7] The electrolyte is typically a solution of tetraethylammonium tetrafluoroborate in acetonitrile or propylene carbonate, restricting the use of EDLCs at higher operating temperatures.

Ionic liquids (ILs) have received a significant a degree of attention as an alternative to organic electrolytes, not only for EDLCs[8,9] but also for lithium ion batteries.[10–13] They are considered to be less hazardous than conventional electrolytes due to their non-flammable nature and the fact that they tend to exhibit negligible vapour pressures.[9,14]

ILs are salts with relatively low melting temperatures (typically <100ºC)[8,13] which is a consequence of the weak interactions between their constituent ions. Typically the cations and anions found in ILs are mismatched in terms of size and frequently display some degree of charge delocalization.[15,16] The structure of these components and their degree of coordination have substantial influence over the physical properties of ILs, with the nature and relative sizes of the ions being known to strongly influence viscosity.[8,17,18] This in turn affects ionic conductivity, which is a crucial parameter in the design of EDLCs as it has a profound influence

on the equivalent series resistance (ESR) of the cells. For example, it is known that ILs containing the bis(trifluoromethanesulfonyl) imide ([Tf_2N]) anion exhibit relatively low viscosities and wide electrochemical stability windows (ESWs). This has been attributed to the partially delocalized charge in the anion which reduces the strength of anion-cation interactions by imparting flexibility into the structure.[19] In addition it has been demonstrated that [Tf_2N] containing ILs can form a stable passivating layer that prevents corrosion of the aluminum current collectors' surface.[20]

A wide ESW is a characteristic frequently associated with ILs, which is also of benefit to their application as EDLC electrolytes. The energy stored in an EDLC, *E*, can be determined using the relationship $E = \frac{1}{2} CV^2$ where *C* represents the cell capacitance and *V* the operating voltage of the cell. The maximum power output, P_{max}, is governed by the relationship, $P_{max}=V^2/(4 \cdot ESR)$ where ESR represents the equivalent series resistance of the device[1]. Therefore the operating voltage, which is limited by the electrochemical stability of the electrolyte, significantly influences the energy and power densities attainable in EDLCs.

Consequently, one of the most widely studied ILs for use in EDLCs is *N*-butyl-*N*-methyl pyrrolidinium bis(trifluorosulfonyl) imide ([Pyr_{14}][Tf_2N]) with several studies demonstrating stable cycling at a remarkably wide operating voltage of 3.6 V.[9,21–24] However, due to the high viscosity and relatively poor conductivity of [Pyr_{14}][Tf_2N] it is mainly operated at elevated temperatures (in the region of 60 ºC), and suffers from limited power capability at room temperature.

An alternative family of ILs that has been identified as potentially useful electrolytes are those based on the trialkylsulfonium cation (S-ILs), which when coupled with the [Tf_2N] anion, display relatively low viscosities and high ionic conductivities.[25–29] A simple example of this is

trimethyl sulfonium [Tf_2N] ([S_{111}][Tf_2N]) which has been investigated for use as an EDLC electrolyte at elevated temperatures (50 ºC and 80 ºC).[30] Despite possessing a melting temperature of 45.5 ºC, this IL was shown to exhibit specific capacitances as high as 140 F g^{-1} at 50 ºC in a system using microporous activated carbon electrodes.

In order to enable operation at lower temperatures and to improve power capabilities, ILs are frequently employed as the conducting salt in an organic-based electrolyte. Concentrated solutions exhibiting high conductivity, low viscosity and wide ESWs can be achieved in such mixtures, with stable cycling at an operating voltage of 3.5 V having been demonstrated using a 1:1 (by wt.) mixture of [Pyr_{14}] [Tf_2N] with propylene carbonate.[31]

The relatively high melting temperature of [S_{111}][Tf_2N] has resulted in the majority of studies that explore the use of S-ILs as EDLC electrolytes to date, focusing on mixtures of this IL with organic solvents such as propylene carbonate,[28,32,33] and more recently the development of deep eutectic solvent mixtures with formamide and trifluoroamide.[34] Despite the former having reduced volatility and flammability in comparison with conventional electrolytes, safety during operation at elevated temperatures remains a concern.

The behavior of neat [S_{222}][Tf_2N] in an EDLC has been previously shown to exhibit good performance in cyclic voltammograms over an operating potential of 2 V, and was reported to display a specific capacitance of 244 F g^{-1} using mesoporous activated carbon electrodes in a flexible cell.[27]

In a recent investigation we reported that two S-ILs ([S_{221}] [Tf_2N] and [S_{222}] [Tf_2N]) performed substantially better, in terms of specific capacitance and internal resistance, than ILs that contained slightly larger ammonium based cations when coupled with several mesoporous

carbon electrodes.[29] The small cation size results in ILs with a relatively low viscosity (and high ionic conductivity) and allows for a greater packing density of ions at the electrode surface.

In this current work we report on the behavior of neat S-ILs in EDLCs operating at room temperature, and investigate the influence that cation structure has on cell performance. Cell operating potentials were determined for each IL using the same microporous activated carbon used to investigate EDLC performance and importantly, the asymmetry of the operating potential was taken into account during EDLC assembly by altering the mass loadings of active material on each electrode. Several physical and electrochemical properties of ILs consisting of diethylmethyl sulfonium [S_{221}], triethyl sulfonium [S_{222}], and dimethylpropyl sulfonium [S_{223}] cations paired with the [Tf_2N] anion are reported alongside their performance in EDLCs. For comparative purposes, all characterizations were also carried out using [Pyr_{14}] [Tf_2N], a relatively established IL electrolyte.[35]

Material and Methods

The ionic liquids used in this study were purchased from Io-Li-Tec GmbH (Germany) and had a minimum stated purity of > 99%. Chart 1 illustrates the structure of the ions contained in these ILs along with the abbreviated name used throughout this report.

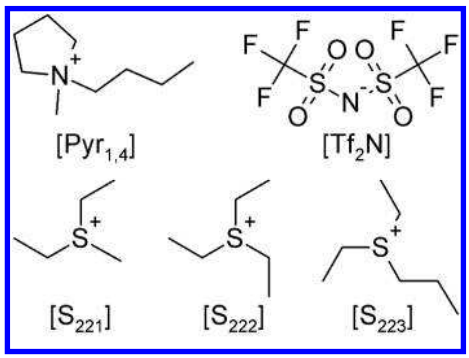

Chart 1. Schematic structure of the constituent ions in the ionic liquids under study. *N*-butyl-*N*-methylpyrrolidinium [Pyr_{14}], bis(trifluoromethanesulfonyl) imide [Tf_2N], diethylmethyl sulfonium [S_{221}], triethyl sulfonium [S_{222}], and dimethylpropyl sulfonium [S_{223}].

Prior to characterisation or cell assembly, ILs were vigorously stirred under heating for several hours in an argon filled glovebox (H_2O <0.1 ppm, O_2 <0.1 ppm). The moisture content of all ILs used in these experiments was determined to be less than 10 ppm using Karl Fischer titration (KF899 Coulometer, Metrohm).

Physicochemical Characterisation. Thermal stability was determined using thermogravimetric analysis (TGA/DSC1, Mettler Toledo). Roughly 10 mg of each sample was heated in an aluminium pan from room temperature to 600ºC at a rate of 10ºC min^{-1} under nitrogen flowing at 50 cm^3min^{-1}.

Differential scanning calorimetry was carried out using a Mettler Toledo DSC1 with liquid nitrogen cooling. Roughly 10 mg of each sample was sealed in an aluminium pan in an argon filled glovebox. Samples were cooled under a nitrogen atmosphere to -100 ºC at a rate of 10 ºC min^{-1}, held at this temperature for 1 hour before heating to 100 ºC at the same rate.

Density and viscosity measurements were performed with a thermoregulated digital densimeter/viscometer (SVM 3000, Anton Paar K.G.).

Ionic conductivity was determined using the impedance method with a Modulab XCM (Solartron) over a frequency range of 100 kHz-10 mHz. The cell constant between two freshly polished platinum electrodes was determined before each experiment using a standard KCl solution.

EDLC assembly and electrochemical characterisation. EDLC electrodes were produced by mixing the activated carbon material (S_{BET} = 2,120 m^2 g^{-1}) with a conductive carbon black (Super C65) and polymer binder (KynarFlex® 2801) in an 80/10/10 ratio by mass. Homogeneous

slurries of this mixture with acetone was spread to varying wet film thicknesses on 15 μm thick aluminium foil using a micrometer adjustable gap paint applicator. Sheets were then dried under vacuum and punched into individual electrodes 12 mm in diameter. The average mass loading of electrodes was in the region of 1.0-2.5 mg.

Two-electrode button cells (2016) were assembled using stainless steel spacers, carbon based electrodes and glass fibre filter paper separator (GF/F, Whatman). The separator was soaked with the IL under study and the cell components were then placed under vacuum in the glovebox antechamber for roughly 5 minutes to encourage the impregnation of the electrolyte into the electrode porosity. Cells were then crimped closed inside the glovebox.

In order to evaluate the electrochemical stability window of the ILs in EDLCs we used counter electrodes with at least twenty times the mass of the conventional working electrodes using the same composition as described above with PTFE (Teflon 30-N) as the polymer binder. This produced self-supporting electrodes 12.6 mm in diameter that were roughly 0.5 mm thick. Cyclic voltammetry was performed on these asymmetric cells from the OCP to 0.5V four times at 5 mVs^{-1}. The window was then increased in 0.1V increments to a maximum of 2.0V. The limit was defined by the lowest potential to have at least 97 % coulombic efficiency. This was repeated using fresh cells for the cathodic limit from 0 to -1.0V initially, increasing in 0.1V increments to a maximum of -2.5V. Four cycles were performed in each potential window and different cells were used for positive and negative sweeps. The combined limits defined the operating potential of the IL. Cyclic voltammetry was carried out using a Solartron Analytical 1470E Multichannel Potentiostat/Galvanostat.

Cells were also cycled Galvanostatically between 0 V and the operating voltage at various rates between 0.1 and 10 Ag^{-1} using a Maccor 4000M cell test system. Electrochemical

impedance spectroscopy (EIS) was performed on the EDLCs at the open circuit potential using a 10mV perturbation over the frequency range 300 kHz to 10 mHz. Specific capacitance values are expressed based on cell capacitance and the combined mass of active material unless stated otherwise.

In the case of cyclic voltammetry experiments the specific capacitance, C (Fg^{-1}), was determined by considering the quantity of charge delivered during discharge, $\int i.dt$ (C), the operating potential window, U (V), and the mass of active materials in both electrodes, m (g) as shown in Equation 1 below.

$$C = \frac{\int i \cdot dt}{U \cdot m} \quad (1)$$

For Galvanostatic measurements, the capacitance was determined from the current, i (A) and the slope of the discharge curve (dV/dt) after any "iR drop" was observed as shown in Equation 2 below.[35]

$$C = \frac{i}{{}^{dV}/_{dt} \cdot m} \quad (2)$$

Cell capacitance determined by electrochemical impedance spectroscopy was determined using Equation 3 where f represents the perturbation frequency (10mHz) and Z_{imag} the imaginary component of the impedance at this frequency.

$$C_{EIS} = \frac{-1}{2\pi f Z_{imag} \cdot m} \quad (3)$$

Associated values of specific energy, E_{ave} ($Wh\ kg^{-1}$), and specific power, P_{ave} ($W\ kg^{-1}$), over the duration of the discharge, t_d (s), were determined from Equations 4 and 5 respectively.[35]

$$E_{ave}[Wh\ kg^{-1}] = i \cdot \int \frac{V}{m \cdot 3.6} \cdot dt_d \quad (4)$$

$$P_{ave}[W\ kg^{-1}] = \frac{E_{ave} \cdot 3600}{t_d} \quad (5)$$

Results and Discussion

Thermal behavior. Table 1 lists the melting and decomposition temperatures of the ILs alongside that of $[Pyr_{14}][Tf_2N]$ for comparison. It is clear that the onset of decomposition of the S-ILs is substantially reduced in comparison with $[Pyr_{14}][Tf_2N]$ which is thermally stable up to a temperature of 445 ºC. There is little difference between the thermal stabilities of the S-ILs, however the onset of decomposition can be seen to increase with decreasing cation size.

Table 1. Physicochemical properties of the ILs $[Pyr_{14}][Tf_2N]$, $[S_{221}][Tf_2N]$, $[S_{222}][Tf_2N]$ and $[S_{223}][Tf_2N]$ at 25 ºC and melting and decomposition temperatures.

	T_d (ºC)[a]	T_m (ºC)	ρ (g cm^{-3})	η (mPa s)	σ (mS cm^{-1})	Λ (S cm^2 mol^{-1})
$[Pyr_{14}][Tf_2N]$	445	-6.5	1.40	78.0	3.0	0.913
$[S_{221}][Tf_2N]$	295	-11.7	1.50	40.6	6.7	1.708
$[S_{222}][Tf_2N]$	290	-17.6	1.46	33.7	7.3	1.995
$[S_{223}][Tf_2N]$	280	-6.4	1.42	37.7	5.5	1.596

[a] T_d represents the onset of thermal decomposition determined by TGA (Heat flow curves for the TGA experiments can be seen Figure S 1 in the Supplementary Information.)

The DSC traces of the ILs are presented in Figure 1 which shows substantially different phase behavior between the S-ILs. On heating $[S_{221}]$ $[Tf_2N]$ exhibits a solid-solid phase transition at -20.4 ºC before melting at -11.7 ºC. $[S_{222}]$ $[Tf_2N]$ appears to exist in the form of a supercooled liquid at -100 ºC, which then undergoes cold crystallization at -58.1 ºC, observed as an exothermic peak. On further heating the sample undergoes two further solid-solid transitions at -32.9 and -10.8 ºC before melting at -6.4 ºC. $[S_{223}][Tf_2N]$ trace shows one baseline change at -68.0 ºC which seems to be the glass transition (T_g), however, this change occurs over a wide temperature range and it is difficult conclusively identify this as the glass transition, after this, it

is possible to observe one small exothermic peak at -47.9 ºC which could be related to a cold crystallization. The melting of this liquid is observed at -6.4 ºC.

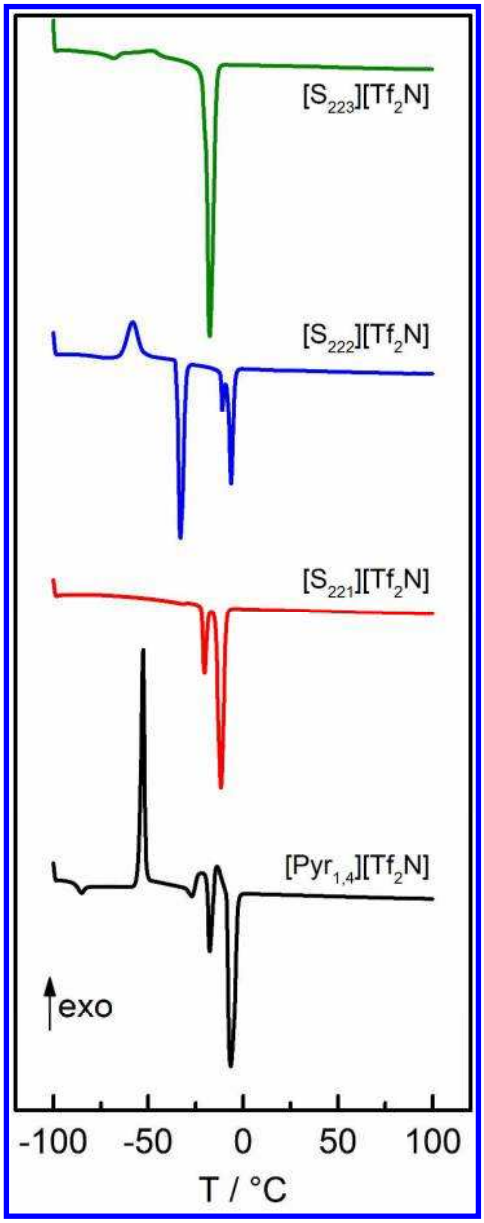

Figure 1. Differential scanning calorimetry traces of $[Pyr_{14}][Tf_2N]$ (black line), $[S_{221}][Tf_2N]$ (red line), $[S_{222}][Tf_2N]$ (blue line) and $[S_{223}][Tf_2N]$ (green line) (from bottom to top).

Physicochemical properties. Figure 2 shows the densities of $[Pyr_{14}][Tf_2N]$ and the S-ILs over a range of temperatures. The densities follow a linear dependence with temperature over the range studied, and is seen to decrease with increasing cation size; the values found are in in good

agreement with the literature.[36] At 25 ºC, $[S_{222}][Tf_2N]$ and $[S_{223}][Tf_2N]$ have densities 2.7% and 5.5% greater than $[S_{221}][Tf_2N]$, and in turn, $[S_{223}][Tf_2N]$ has a density 2.7% greater than $[S_{222}][Tf_2N]$. The decrease of density as a function of increased alkyl chain length has been discussed by several groups studying ILs containing similar cations such as the tetraalkylammonium group of cations.[26,36–38]

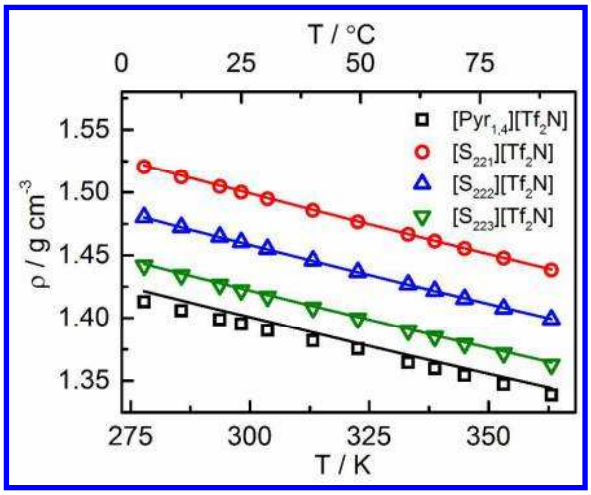

Figure 2. Experimental density (symbols) and estimated density (lines) of the ILs $[Pyr_{14}][Tf_2N]$ (black square and line), $[S_{221}][Tf_2N]$ (red circle and line), $[S_{222}][Tf_2N]$ (blue up triangle and line) and $[S_{223}][Tf_2N]$ (green down triangle and line) at a range of temperature.

Using the extended version of density estimation by Gardas and Coutinho (Equation 6),[39] from Ye and Shreeve equation,[40] it is possible to estimate the liquids density over the studied range of temperature:

$$\rho = \frac{M}{NV(a+bT+cp)} \cdot 10^{24} \qquad (6)$$

where ρ is the calculated density (g cm^{-3}), M is the molecular weight (g mol^{-1}), V is the molecular volume (Å^3), T is the temperature (K) and p is the pressure (MPa). The coefficients a, b and c are 0.8005, 6.652 10^{-4} K^{-1} and -5.919 10^{-4} MPa^{-1}. M and V for the ILs presented here can be seen in Table S 1, in the Supplementary Information.

Although the model is suggested for use between temperatures of 288.15 and 353.15 K, we applied it over the experimental temperature range (277.85 to 363.15 K), and found that the calculated densities are in good agreement with the experimental values. The absolute average relative deviations for the ILs $[Pyr_{14}][Tf_2N]$, $[S_{221}][Tf_2N]$, $[S_{222}][Tf_2N]$ and $[S_{223}][Tf_2N]$ are 0.46%, 0.044%, 0.024% and 0.096%, respectively. The trend shows that increasing size of sulfonium cation results in reduced density, despite the larger ions having greater mass.

Figure 3a shows the variation in viscosity with temperature for the four ILs. $[Pyr_{14}][Tf_2N]$ presents the highest viscosity amongst the ILs studied at each temperature. The S-ILs present fairly similar values of viscosity at each temperature studied. For example, at 25 ºC (298 K) $[S_{221}][Tf_2N]$, $[S_{222}][Tf_2N]$ and $[S_{223}][Tf_2N]$ present viscosities of 40.6, 33.7 and 37.7 mPa s. There is no clear trend seen in viscosity with alkyl chain length. The lines in Figure 3a represent the best fits by the Vogel-Tammann-Fulcher (VTF) equation[41] for the ILs viscosities, $\eta = \eta_0 e^{B/T-T_0}$, where η_0, B and T_0 are adjustable parameters, given in Table S 2, in Supplementary Information. The relationship B/T_0 is related to the liquid fragility, or the manner in which transport properties vary with changing temperature. Low B/T_0 indicates that the liquid is strong and its transport properties are influenced to a lesser extent with changes in temperature than liquids associated with a high value of B/T_0. It is important to clarify that the fragility analysis is often performed near the T_g, and changes in the fit profile should be considered at lower temperatures than the range presented here.[42,43] The viscosity VTF fit indicates that the four ILs studied here present similar fragility as they present similar values of B/T_0, *i.e.* the transport properties experience similar changes when the temperature is changed.

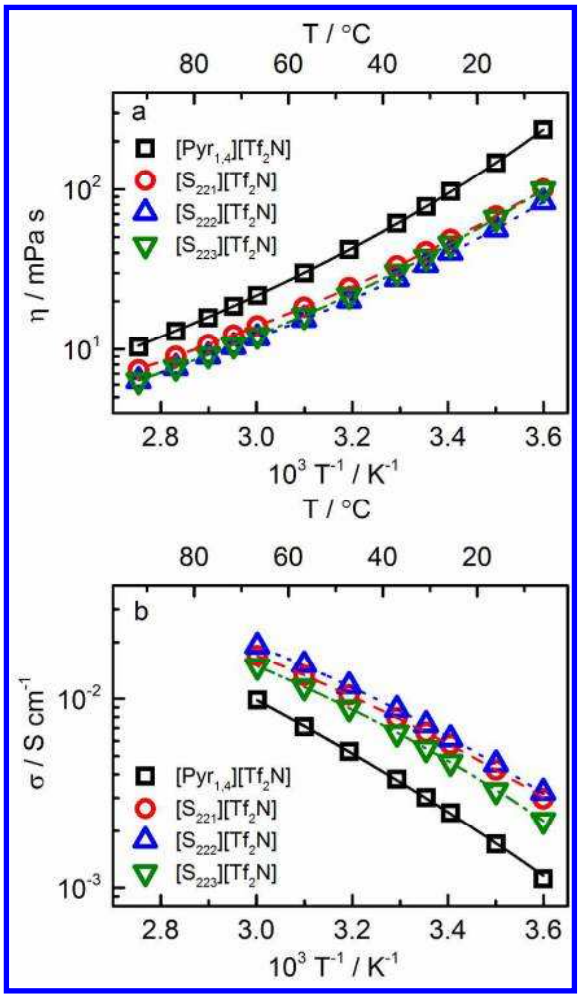

Figure 3. Arrhenius-like plot of (a) viscosity and (b) ionic conductivity for $[Pyr_{14}][Tf_2N]$ (black square), $[S_{221}][Tf_2N]$ (red circle), $[S_{222}][Tf_2N]$ (blue up triangle) and $[S_{223}][Tf_2N]$ (green down triangle). Lines represent the best fits of the VTF equations for viscosity and ionic conductivity.

Figure 3b shows the ionic conductivity of the four ILs as function of temperature. As is well established, ionic conductivity is seen to increase with temperature. The S-ILs present significantly higher ionic conductivities than $[Pyr_{14}][Tf_2N]$ at each temperature studied. As with the case of viscosity, the ionic conductivity does not display a simple relationship with alkyl chain length, and surprisingly $[S_{223}][Tf_2N]$ is seen to present the lowest values of conductivity of the S-ILs, which is a feature that does not correlate with the viscosity measurements. At 25 ºC (298 K), $[S_{221}][Tf_2N]$, $[S_{222}][Tf_2N]$ and $[S_{223}][Tf_2N]$ present 6.7, 7.3 and 5.5 mS cm^{-1} which are

in good agreement with the available literature.[25,26] The VTF fits for ionic conductivity are the lines presented in Figure 3b, the equation for ionic conductivity VTF fit is $\sigma = \sigma_0 e^{-B/T-T_0}$, where σ_0, B and T_0 are the adjustable parameters, which can be seen in Table S 2, in Supplementary Information. The values of B/T_0 derived for the S-ILs are slighter lower for the ionic conductivity fit in comparison with the viscosity fit.

Figure 4 shows the molar ionic conductivity (Λ) as a function of fluidity (η^{-1}, inverse viscosity). In addition, Figure S 2 presents a conventional Walden plot, (log ionic conductivity as function of log fluidity (Poise^{-1})); in this plot the ideal line for dilute KCl aqueous solution has a slope of unity.[43] Λ was calculated considering the density at each temperature and the concentration of ions. $[Pyr_{14}][Tf_2N]$, $[S_{221}][Tf_2N]$, $[S_{222}][Tf_2N]$ and $[S_{223}][Tf_2N]$ present concentrations of 3.30, 3.89, 3.66 and 3.44 mmol cm^{-3} at 25 ºC (298 K) respectively. The slope of the linear fit of these points is related with the liquid ionicity; a steeper gradient signifies larger ionicity, indicating that more ions are free to participate in the conduction process. The parameters from the linear fits can be seen in Table S 3. The ILs $[Pyr_{14}][Tf_2N]$, $[S_{221}][Tf_2N]$ and $[S_{222}][Tf_2N]$ present similar slopes and therefore exhibit similar ionicities. On the other hand, $[S_{223}][Tf_2N]$ presents a substantial deviation from the behavior seen in other ILs indicating that this IL tends to form more aggregates that result in decreased molar ionic conductivity at the same fluidity.

However, one must consider that even with a lower ionicity, $[S_{223}][Tf_2N]$ presents a higher molar ionic conductivity than $[Pyr_{14}][Tf_2N]$ when compared at the same temperature. It may be the case that the charge distribution around the $[S_{223}]$ cation differs significantly from that of $[S_{221}]$ and $[S_{222}]$ due to the propyl chain resulting in more interactions with other ions. These

interactions produce a greater quantity of neutral aggregates when compared with the other ILs, resulting in a lower ionicity.

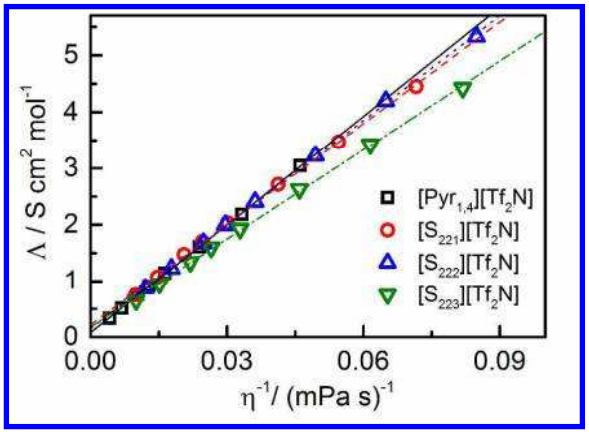

Figure 4. Relationship between molar ionic conductivity and fluidity (Λ vs. η^{-1}) of $[Pyr_{14}][Tf_2N]$ (black square), $[S_{221}][Tf_2N]$ (red circle), $[S_{222}][Tf_2N]$ (blue up triangle) and $[S_{223}][Tf_2N]$ (green down triangle). Lines are the linear fit.

Electrochemical performance. The electrochemical stability of the ILs was investigated in order to ascertain stable operating potentials for EDLCs. It has been shown that electrolytes can decompose over much narrower potential windows when coupled with activated carbon electrodes in comparison with those obtained in conventional three-electrode setups using planar electrodes.[44] For this reason we assembled asymmetric cells where the counter electrode had a far greater capacitance than the working electrode, and performed cyclic voltammetry (CV) at 5 mVs^{-1} over increasingly wide potential windows in either the positive or negative direction. Figure 5 shows how the coulombic efficiency of the cells vary with potential (symbols and left y axis) and present cyclic voltammograms of the cells measured at the potential limits defined by a coulombic efficiency of at least 97% (lines and right y axis).

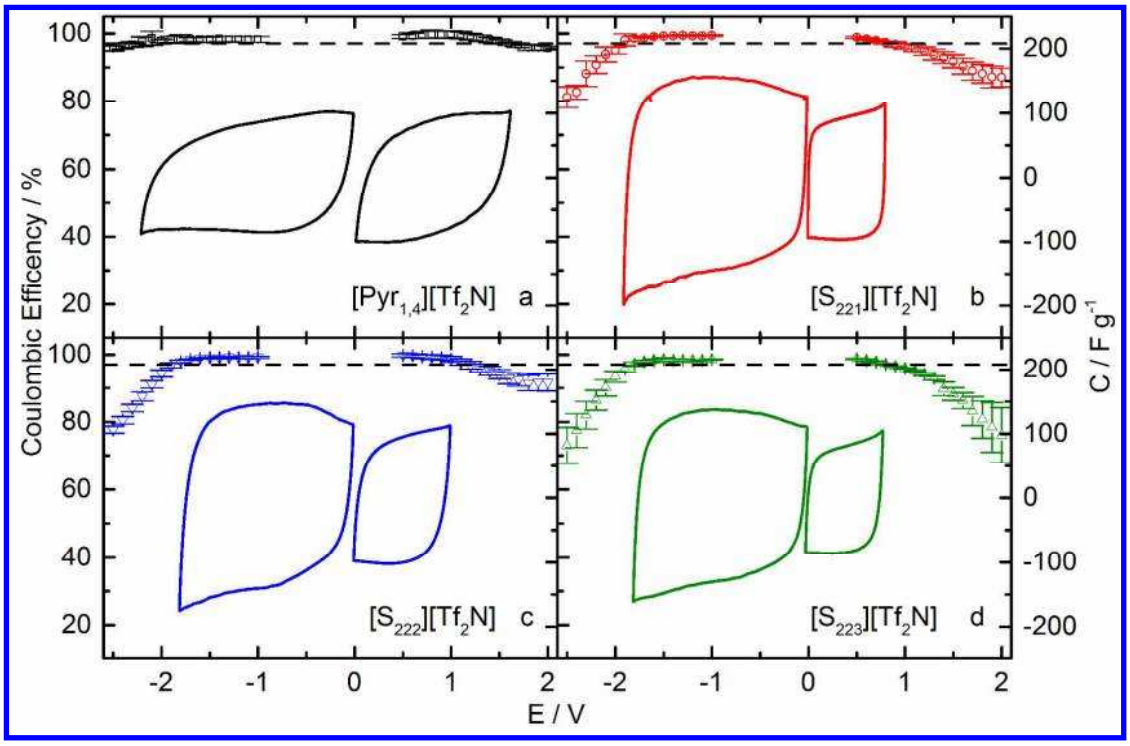

Figure 5. Operating potential determination using cyclic voltammetry. Coulombic efficiency (symbols, left) of cells used in the determination of anodic/cathodic limits. Cells cycled from OCP to 0.5V, then in 0.1V increments to 2.0V. Limit defined by the potential at which 97% efficiency was observed. Fresh cells used to determine the cathodic limit, cycling from OCP to -1.0V initially and in 0.1V increments to -2.5V. Cyclic voltammograms of these "half-cells" expressed in the form of specific capacitance (lines, right) for the defined potential limits.

At the determined operating potential limits (at least 97% efficiency), Figure 5 presents the cyclic voltammograms of the cells obtained at a sweep rate of 5 mVs^{-1}. Figure 5a shows the behavior of cells using $[Pyr_{14}][Tf_2N]$ with a limit of 1.6 V for the positive electrode and -2.2 V for the negative electrode. The asymmetry of these potential windows is typical of $[Pyr_{14}][Tf_2N]$, and the determined operating potential is similar to those found in other studies.[21,35,45]

The operating windows of the S-ILs are markedly asymmetric, even more so than that observed for $[Pyr_{14}][Tf_2N]$. The positive limits for the S-ILs are substantially smaller than that of $[Pyr_{14}][Tf_2N]$ which could be a result of a lower charge density associated with the pyrrolidinium

cation. The more rectangular form of the CVs exhibited by the S-ILs in Figure 5 when compared with $[Pyr_{14}][Tf_2N]$ indicates reduced resistances associated with these electrolytes.

As could be expected, the operating potential of $[S_{223}][Tf_2N]$ was the lowest of those tested at 2.6 V, which can be attributed to the cleavage of the pendant methyl group occurring at the lower potential. $[S_{222}][Tf_2N]$ was found to be more stable than $[S_{221}][Tf_2N]$ (with operating potentials of 2.8 V and 2.7 V respectively), possibly due to the more localized charge density of the smaller cation. The symmetry and more delocalized charge of the $[S_{222}]$ cation may render this IL slightly more stable than $[S_{221}][Tf_2N]$ and $[S_{223}][Tf_2N]$ with respect to potential.

Due to the asymmetry of the potential windows, different mass loadings on the electrodes are required to ensure that cells are not operating in a region that results in electrolyte decomposition.[46] The operating limits and mass loading ratios derived from the CVs in Figure 5 are listed in Table 2.

Table 2. Operating potential limits and mass loading ratios determined using cyclic voltammetry. Limits determined at a coulombic efficiency of 97% from experiments performed at 25ºC using a sweep rate of $5mVs^{-1}$ (Figure 5).

	Negative limit (V (*vs* OCP))	Positive limit (V (*vs* OCP))	m_+/m_-
$[Pyr_{14}][Tf_2N]$	-2.2	1.6	1.38
$[S_{221}]][Tf_2N]$	-1.9	0.8	2.38
$[S_{222}][Tf_2N]$	-1.8	1.0	1.80
$[S_{223}][Tf_2N]$	-1.8	0.8	2.25

Initially the ratios used were determined by balancing the amount of charge delivered during the discharge step on each electrode according to the equation 7 below.

$$\frac{m_+}{m_-} = \frac{q_-}{q_+} \quad (7)$$

Where $m_\pm$ represents the mass loading of active material on the positive/negative electrode and $q_\pm$ represents the quantity of charge delivered from the positive/negative limit back to the open circuit potential (OCP). As the capacitive response at negative potentials is significantly larger than that seen at positive potentials, balancing the charge in this manner resulted in relatively large mass loading ratios of 4.5, 2.25 and 3.3 for $[S_{221}][Tf_2N]$, $[S_{222}][Tf_2N]$ and $[S_{223}][Tf_2N]$ respectively. (As the magnitude of the capacitances using $[Pyr_{14}][Tf_2N]$ are similar (see Figure 5a), this method resulted in a mass loading ratio of 1.45 which is similar to that reported in other studies.[35,46] However as EDLCs assembled with these ratios exhibited significant electrolyte decomposition during cyclic voltammetry at 5 mV s^{-1} (see Figure S 3 in Supporting Information) and remarkably low coulombic efficiencies (*ca.* 80%) it was decided to simply use the ratio of negative to positive limit indicated in Table 2.

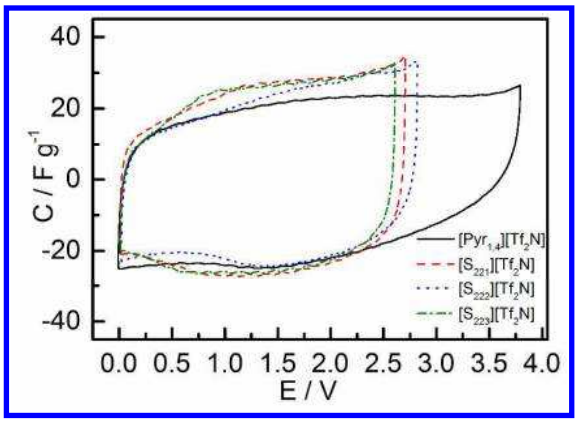

Figure 6. Cyclic voltammograms of EDLCs using different IL electrolytes. $[Pyr_{14}][Tf_2N]$ (black full line), $[S_{221}][Tf_2N]$ (red dashed line), $[S_{222}][Tf_2N]$ (blue dotted line) and $[S_{223}][Tf_2N]$ (green dash dotted line). Experiments were performed at 25ºC using a sweep rate of 5 mVs^{-1}.

Figure 6 shows typical rectangular CVs obtained for EDLCs using each of the ILs at a sweep rate of $5mVs^{-1}$. The lack of significant peaks in Figure 6 indicates that no faradaic reactions

occur over the operating potentials used, and that there is very little difference between the behavior of $[S_{221}][Tf_2N]$ and $[S_{223}][Tf_2N]$. It is apparent that the S-ILs exhibit slightly larger specific capacitances during discharge than $[Pyr_{14}][Tf_2N]$. This may be a result of the smaller cation size enabling a greater density of charge displacement at the electrode surface or permitting access to narrower pores in the electrode. The larger specific current associated with the charging process may also be an artifact of the relatively slow sweep rate used; at such slow rates the increased conductivity of the S-ILs could enhance the effects of competing "self-discharge" processes. These background and/or leakage currents may also be responsible for the limited anodic stability determined using an arbitrary value of coulombic efficiency. To investigate the effect of operation at different rates, CVs were collected at different sweep rates and are presented in Figure 7. (For comparative purposes an operating voltage of 2.5V was used for all cells.)

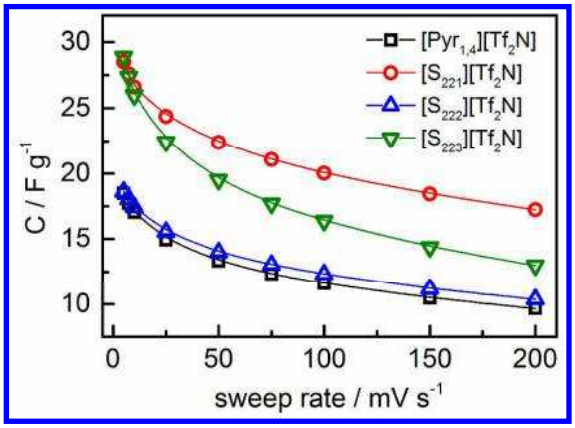

Figure 7. Comparison of specific capacitance determined using cyclic voltammetry at different sweep rates. $[Pyr_{14}][Tf_2N]$ (black squares), $[S_{221}][Tf_2N]$ (red circles), $[S_{222}][Tf_2N]$ (blue up triangles) and $[S_{223}][Tf_2N]$ (green down triangles). Experiments were performed between 0 and 2.5 V at 25ºC using sweep rates between 5 and 200 mVs^{-1}.

As can be expected from their physical properties, the S-ILs show improved rate performance when compared with $[Pyr_{14}]$ $[Tf_2N]$, however this is only marginal in the case of $[S_{222}][Tf_2N]$. At

the lowest rate studied, $[S_{223}][Tf_2N]$ results in a slightly larger specific capacitance than $[S_{221}][Tf_2N]$, however as the rate increases $[S_{221}][Tf_2N]$ is seen to perform better, and the disparity between their specific capacitances is seen to increase with increasing rate. This may be a result of the $[S_{223}][Tf_2N]$ ion being able to make use of smaller pores in the electrode but only if sufficient time is available during charging for the optimal rearrangement of ions at the electrode surface.

$[S_{221}][Tf_2N]$ is seen to result in greater specific capacitances than $[S_{222}][Tf_2N]$ at all of the rates studied which was also shown in our previous study using mesoporous carbon electrodes in symmetrical cells.[29] It is rather surprising that $[S_{222}][Tf_2N]$ performs so poorly in comparison with $[S_{221}][Tf_2N]$ and $[S_{223}][Tf_2N]$ considering that it displays a higher conductivity and lower viscosity. In fact, despite the significant differences in physical properties and ion size, the performance of $[S_{222}][Tf_2N]$ most closely resembles that of $[Pyr_{14}][Tf_2N]$. It may be that the aspect ratios of the other cations permit tighter packing at the electrode surface, the utilization of narrower pores or a reduced distance between the charge center and the electrode; all of these would result in a greater degree of charge being displaced in the electrode resulting in increased capacitance. As the activated carbon used in the electrodes is highly microporous (see Figure S 4 in Supporting Information) it is possible that a fraction of pores inaccessible to the $[S_{222}]$ ion are available to the smaller $[S_{221}]$ ion, or are able to be partially occupied by the $[S_{223}]$ ion which is slightly larger but has a different aspect ratio. It is also likely that the physical properties observed in the bulk liquid are substantially different to that seen when ions are constricted within the pores of an electrode and it has been shown that different charging mechanisms occur in porous electrodes when compared with ideal planar electrodes.[47–49]

At 5 mVs^{-1} all of the cells exhibit a coulombic efficiency of *ca.* 90% which rises to over 98% for sweep rates greater than $50mVs^{-1}$. (At 200 mVs^{-1} the average coulombic efficiency of the cells was found to be 99.3%.) This highlights the compromises that are present in the design of EDLCs and the majority of electrochemical energy storage devices; increased electrolyte conductivity reduces the internal resistance of devices but can result in increased self-discharge and diminished efficiency at low rates.

A wider range of charge/discharge rates was explored using galvanostatic cycling at specific currents between 0.1 and 10 Ag^{-1}. The results are presented in Figure 8.

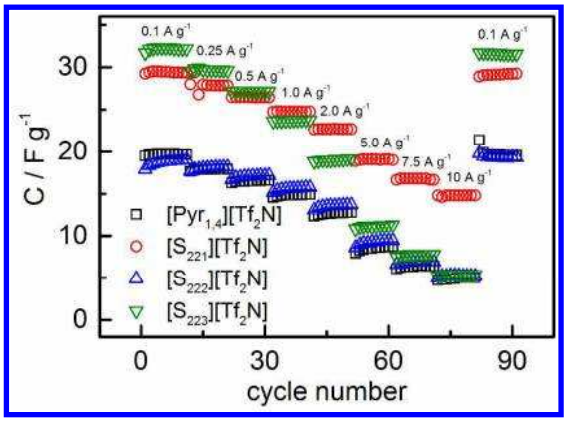

Figure 8. Comparison of specific capacitance determined using galvanostatic charge/discharge cycling at different rates. $[Pyr_{14}][Tf_2N]$ (black squares), $[S_{221}][Tf_2N]$ (red circles), $[S_{222}][Tf_2N]$ (blue up triangles) and $[S_{223}][Tf_2N]$ (green down triangles). Experiments were performed at 25ºC using rates between 0.1 and 10 Ag^{-1}.

Considering the discharge time of the cells, the range of sweep rates in Figure 7 corresponds to values of specific current up to roughly 2 Ag^{-1} in Figure 8. It is clear that $[S_{222}][Tf_2N]$ behaves in a similar way to $[Pyr_{14}][Tf_2N]$ at all of the rates investigated. At a rate of $0.1Ag^{-1}$ $[S_{222}][Tf_2N]$ produces a smaller specific capacitance than even $[Pyr_{14}][Tf_2N]$ which could be a result of relatively high background/leakage currents arising from the higher conductivity of this IL.

At rates below 1 Ag^{-1} $[S_{223}][Tf_2N]$ produces a greater specific capacitance than $[S_{221}][Tf_2N]$ which is similar behavior to that observed at 5 mVs^{-1} in Figure 7. This trend is changed at higher

rates with $[S_{221}][Tf_2N]$ producing greater specific capacitances when the specific current is greater than 1 Ag^{-1}. The sharp drop in specific capacitance at rates greater than 2 Ag^{-1} observed for $[S_{223}][Tf_2N]$ was unanticipated considering the degree of capacitance retention seen in Figure 7. At the most aggressive rates used during galvanostatic cycling, $[S_{223}][Tf_2N]$ is seen to behave in a manner more similar to that of $[S_{222}][Tf_2N]$ and $[Pyr_{14}][Tf_2N]$. This may be a result of the lower conductivity of $[S_{223}][Tf_2N]$ when compared with $[S_{221}][Tf_2N]$.

Another explanation for the fact that $[S_{223}][Tf_2N]$ performs well at low rates but poorly at higher rates may be related to the relationship seen in Figure 4 where the existence of aggregated ions in $[S_{223}][Tf_2N]$ is indicated by the significantly lower molar conductivity determined at the same level of fluidity. At low rates it is possible that there is sufficient time during charge and discharge for these coordinated ions to be freed from the aggregates, migrate towards the electrode surface and be involved charge storage through the double layer mechanism. At higher rates there is insufficient time for this process to occur and only the disassociated fraction of ions can participate in charge storage. Simulations suggest that there is no bulk movement of ions in the pores upon polarization, however the degree of ionic coordination changes as ions are exchanged with the bulk electrolyte.[49] In the case of $[S_{223}][Tf_2N]$ it may be that the timescale over which these processes occur overlaps with the discharge times observed during galvanostatic cycling. Therefore at shorter timescales the poorer response of $[S_{223}][Tf_2N]$ may be a result of the greater degree of ionic coordination or stronger interactions being present between these ions when compared to the other Ils studied.

Electrochemical impedance spectroscopy (EIS) measurements were performed on EDLCs using each of the ILs, and the obtained Nyquist plots are presented in Figure 9. Each of the spectra are of similar form, typical of EDLCs with IL electrolytes, that consist of a semicircle at

the high frequency region and a linear region in the low frequency range. In the case of an interface displaying pure capacitive behavior, the spectra at low frequencies is parallel to the imaginary axis. The deviation from vertical, as seen in Figure 9 for all of the ILs, indicates that there is inhomogeneity in the double layer region. This is frequently seen when using porous electrodes and is a result of slow processes occurring at the interface between the electrode and electrolyte such as specific adsorption or the rearrangement of ions and charge redistribution.[50–52]

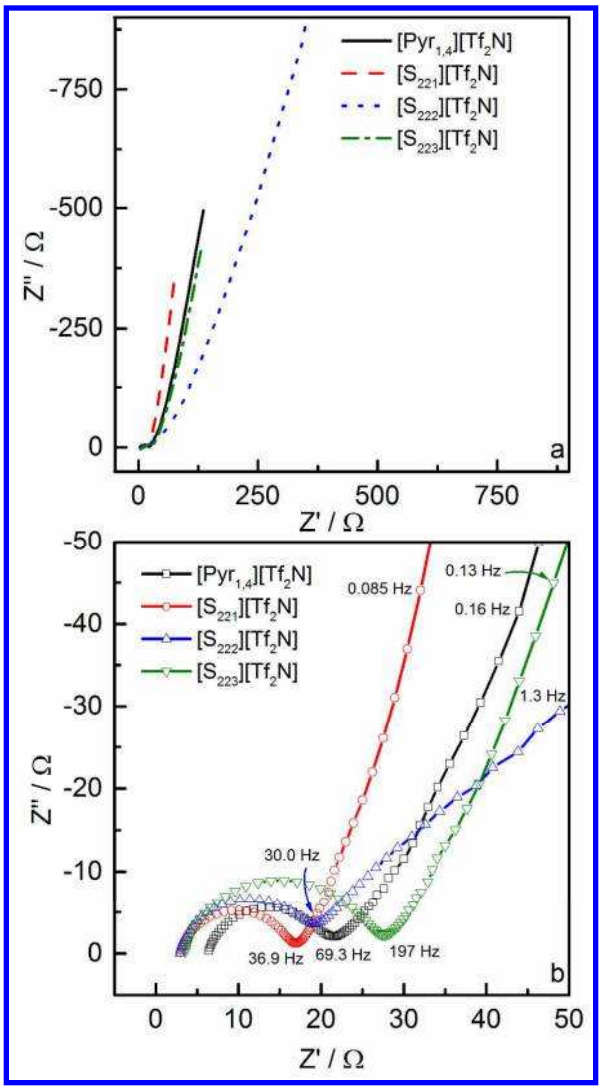

Figure 9. Nyquist plots from electrochemical impedance spectroscopy measurements with magnified inset showing high frequency behavior. $[Pyr_{14}][Tf_2N]$ (full black line and black squares), $[S_{221}][Tf_2N]$ (dashed red line and red circles), $[S_{222}][Tf_2N]$

(dotted blue line and blue up triangles) and $[S_{223}][Tf_2N]$ (dash-dotted green line and green down triangles). Experiments were performed at 25ºC in coin cells using four-point Kelvin connectors.

Characteristic resistances determined from the spectra in Figure 9 alongside values of specific capacitance (determined from the imaginary component of the impedance at 10mHz) are given in Table 3.

Table 3. Cell characteristics determined from electrochemical impedance spectroscopy measurements.

	C_{EIS} / F g^{-1}	R_s / Ω	R_i / Ω
$[Pyr_{14}][Tf_2N]$	15.1	6.4	15.4
$[S_{221}]][Tf_2N]$	22.0	3.0	14.1
$[S_{222}][Tf_2N]$	9.7	3.0	17.2
$[S_{223}][Tf_2N]$	19.1	3.5	22.0

C_{EIS} represents cell capacitance from the spectra at 10mHz, R_s represents the series resistance (identified as the real component of the impedance where the spectra crosses the imaginary axis) and R_i represents the ionic resistance (defined as the diameter of the high-frequency semicircle).

There is a marked difference between the spectra of the S-ILs and that of $[Pyr_{14}][Tf_2N]$. The series resistance (R_s), identified as the real component of the impedance where the spectra crosses the imaginary axis, is substantially greater for $[Pyr_{14}][Tf_2N]$ when compared with the other spectra. This could be expected as this represents the resistance of the electrolyte and $[Pyr_{14}][Tf_2N]$ exhibits a markedly lower conductivity at room temp than the other ILs. The value of series resistance is similar for $[S_{221}][Tf_2N]$ and $[S_{222}][Tf_2N]$ whereas $[S_{223}][Tf_2N]$ is slightly larger. These findings are in rough agreement with the relative ionic conductivity of the ILs since $[S_{221}][Tf_2N]$ and $[S_{222}][Tf_2N]$ present similar ionic conductivities of 6.7 and 7.3 mS cm^{-1} respectively, whereas $[S_{223}][Tf_2N]$ presents a slightly smaller value of 5.5 mS cm^{-1} (Table 1).

The semicircle seen at high frequencies is attributed to the interactions between the pores of the electrode with the ions in the electrolyte.[53] In terms of the S-ILs, the diameter of the semicircle (R_i), is seen to increase with increasing ion size and the value of R_i for $[Pyr_{14}][Tf_2N]$ falls between that of $[S_{221}][Tf_2N]$ and $[S_{222}][Tf_2N]$. As the value of R_i is influenced by the ionic mobility of the electrolyte it can be expected that the conductivity, ion size and degree of coordination between the ions influence this property in a complex manner and that behavior observed in bulk ILs may not be applicable to situations where the ions are constrained by the surfaces of a porous electrode.

The energy and power characteristics of EDLCs were derived from galvanostatic charge discharge experiments at different current densities and are given in Figure 10. The operating voltage of the cells using S-ILs was 2.5 V whereas the cell using $[Pyr_{14}][Tf_2N]$ was operated at 3.6 V to give a better reflection of the capability of this electrolyte. At a current density of 0.1 Ag^{-1}, the highest specific energy is exhibited by $[Pyr_{14}][Tf_2N]$ which could be anticipated due to the substantially larger operating voltage used. At current densities greater than 0.25 Ag^{-1} $[S_{221}][Tf_2N]$ displays higher values of specific energy and specific power despite the limited operating potential. This is due to the smaller resistances associated with the $[S_{221}][Tf_2N]$ cells.

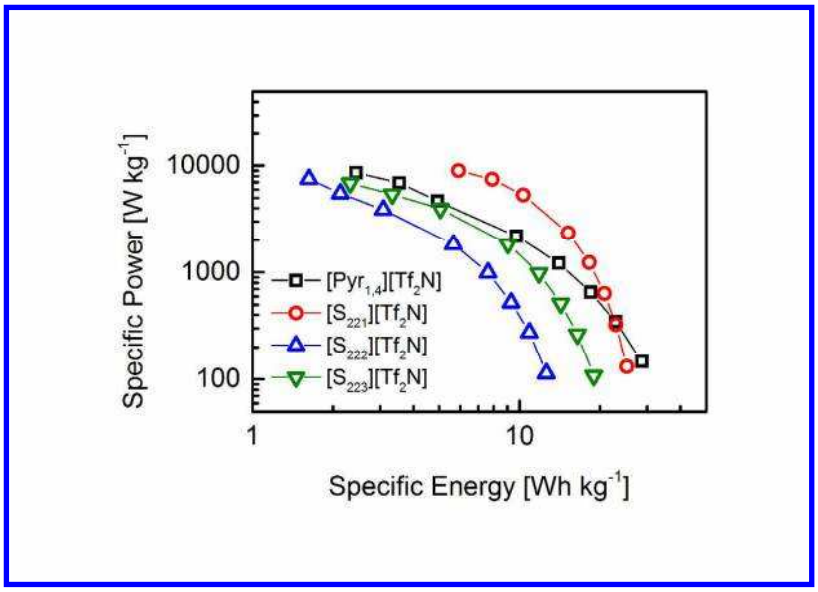

Figure 10. Ragone plot of EDLCs using [Pyr_{14}][Tf_2N] at 3.6V (black line and squares), [S_{221}][Tf_2N] at 2.5V (red line and circles), [S_{222}][Tf_2N] at 2.5V (blue line and up triangles) and [S_{223}][Tf_2N] at 2.5V (green line and down triangles). Values are derived from galvanostatic charge discharge experiments at different current densities.

Figure 10 shows that [S_{221}][Tf_2N] can perform better as an EDLC electrolyte than [Pyr_{14}][Tf_2N] at room temperature despite operating at a lower potential. The behavior of [S_{222}][Tf_2N] and [S_{223}][Tf_2N] in Figure 10 also shows that despite exhibiting several desirable traits (*i.e.* higher ionic conductivity and lower viscosity), enhanced electrochemical stability can outweigh some of the limitations associated with IL electrolytes.

Conclusion

In this work we investigate the behavior of ionic liquids containing sulfonium cations as electrolytes for EDLCs. Physical properties such as viscosity and ionic conductivity were reported over a range of temperatures, as well as their thermal and electrochemical behavior. The S-ILs were shown to exhibit relatively low viscosities and high ionic conductivities (with their relative performance being related to the size and structure of the cation) however they also

exhibited limited electrochemical stability resulting in an operating voltage of 2.5V. The electrochemical performance of the S-ILs was not found to relate to any physical property in a simple manner. For example $[S_{222}][Tf_2N]$ displays the highest ionic conductivity and lowest viscosity, which are desirable traits for an electrolyte, but exhibits comparable performance in terms of specific capacitance with $[Pyr_{14}][Tf_2N]$ which contains a larger cation and exhibits low ionic conductivity and high viscosity.

The unusual behavior of $[S_{223}][Tf_2N]$ which displays relatively high specific capacitances at low rates but substantially diminished performance at higher rates, was attributed to the existence of aggregated ions that are unable to participate in charge storage at higher rates. This ionic coordination is evident when viscosity and conductivity are expressed in the form of a Walden plot where $[S_{223}][Tf_2N]$ displays a significantly different gradient to the other ILs.

In conclusion, this work shows that $[S_{221}][Tf_2N]$ can perform better as an EDLC electrolyte than $[Pyr_{14}][Tf_2N]$ at room temperature despite operating at a lower potential. It is also clear that despite exhibiting desirable traits such as relatively high ionic conductivity and low viscosity, enhanced electrochemical stability can outweigh some of the limitations associated with IL electrolytes in terms of energy and power.

ASSOCIATED CONTENT

Supporting Information. Thermogravimetric analyses of each IL (Figure S 1). Molecular weight and molecular volumes of each IL (Table S 1). VTF fit parameters for the viscosity and ionic conductivity (Table S 2). Molar ionic conductivity and fluidity fit parameters (Table S 3). Walden plot (Figure S 2). Cyclic voltammograms using alternative mass loadings (Figure S 3). Pore size distribution of activated carbon used in EDLC electrodes **(**Figure S 4). This material is available free of charge via the Internet at http://pubs.acs.org.

AUTHOR INFORMATION

Corresponding Authors

**Email: a.rennie@sheffield.ac.uk; peter.hall@sheffield.ac.uk*

Author Contributions

The manuscript was written through contributions of all authors. All authors have given approval to the final version of the manuscript. ‡These authors contributed equally.

ACKNOWLEDGMENT

The authors are indebted to the EPSRC (EP/K021192/1) and FAPESP (09/53199-3) for funding. VLM thanks FAPESP (13/22748-7 and 14/14690-1) for fellowship support. The authors acknowledge Dr. Nédher Sanchez-Ramirez for conducting viscosity and density measurements (FAPESP 14/01987-6).

REFERENCES

(1) Conway, B. E. *Electrochemical Supercapacitors: Scientific Fundamentals and Technological Applications*; Kluwer Academic/Plenum Publishing: New York, 1999.

(2) Simon, P.; Gogotsi, Y. Materials for Electrochemical Capacitors. *Nat. Mater.* **2008**, *7*, 845–854.

(3) Miller, J. R.; Burke, A. F. Electrochemical Capacitors: Challenges and Opportunities for Real-World Applications. *Electrochem. Soc. Interface* **2008**, *17*, 53–57.

(4) Kötz, R; Carlen, M. Principles and Applications of Electrochemical Capacitors. *Electrochim. Acta* **2000**, *45*, 2483–2498.

(5) Hall, P. J.; Mirzaeian, M.; Fletcher, S. I.; Sillars, F. B.; Rennie, A. J. R.; Shitta-Bey, G. O.; Wilson, G.; Cruden, A.; Carter, R. Energy Storage in Electrochemical Capacitors: Designing Functional Materials to Improve Performance. *Energy Environ. Sci.* **2010**, *3*, 1238–1251.

(6) Pandolfo, A. G.; Hollenkamp, A. F. Carbon Properties and Their Role in Supercapacitors. *J. Power Sources* **2006**, *157*, 11–27.

(7) Béguin, F.; Presser, V.; Balducci, A.; Frackowiak, E. Carbons and Electrolytes for Advanced Supercapacitors. *Adv. Mater.* **2014**, *26*, 2219–2251.

(8) Galiński, M.; Lewandowski, A.; Stepniak, I.; Galinski, M.; Lewandowski, A.; Stepniak, I. Ionic Liquids as Electrolytes. *Electrochim. Acta* **2006**, *51*, 5567–5580.

(9) Brandt, A.; Pohlmann, S.; Varzi, A.; Balducci, A.; Passerini, S. Ionic Liquids in Supercapacitors. *MRS Bull.* **2013**, *38*, 554–559.

(10) Koch, V. R.; Nanjundiah, C.; Battista Appetecchi, G.; Scrosati, B. The Interfacial Stability of Li with Two New Solvent-Free Ionic Liquids: 1,2-Dimethyl-3-Propylimidazolium Imide and Methide. *J. Electrochem. Soc.* **1995**, *142*, L116–L118.

(11) MacFarlane, D. R.; Huang, J.; Forsyth, M. Lithium-Doped Plastic Crystal Electrolytes Exhibiting Fast Ion Conduction for Secondary Batteries. *Nature* **1999**, *402*, 792–794.

(12) Lewandowski, A.; Świderska-Mocek, A. Ionic Liquids as Electrolytes for Li-Ion Batteries-An Overview of Electrochemical Studies. *J. Power Sources* **2009**, *194*, 601–609.

(13) Armand, M.; Endres, F.; MacFarlane, D. R.; Ohno, H.; Scrosati, B. Ionic-Liquid Materials for the Electrochemical Challenges of the Future. *Nat. Mater.* **2009**, *8*, 621–629.

(14) Mysyk, R.; Ruiz, V.; Raymundo-Piñero, E.; Santamaria, R.; Béguin, F. Capacitance Evolution of Electrochemical Capacitorswith Tailored nanoporous Electrodes in Pure and Dissolved Ionic Liquids. *Fuel Cells* **2010**, *10*, 834–839.

(15) Welton, T. Room-Temperature Ionic Liquids. Solvents for Synthesis and Catalysis. *Chem. Rev.* **1999**, *99*, 2071–2084.

(16) Buzzeo, M. C.; Evans, R. G.; Compton, R. G. Non-Haloaluminate Room-Temperature Ionic Liquids in Electrochemistry - A Review. *ChemPhysChem* **2004**, *5*, 1106–1120.

(17) Martins, V. L.; Sanchez-Ramirez, N.; Ribeiro, M. C. C.; Torresi, R. M. Two Phosphonium Ionic Liquids with High Li+ Transport Number. *Phys. Chem. Chem. Phys.* **2015**, *17*, 23041–23051.

(18) Sanchez-Ramirez, N.; Martins, V. L.; Ando, R. A.; Camilo, F. F.; Urahata, S. M.; Ribeiro, M. C. C.; Torresi, R. M. Physicochemical Properties of Three Ionic Liquids Containing a Tetracyanoborate Anion and Their Lithium Salt Mixtures. *J. Phys. Chem. B* **2014**, *118*, 8772–8781.

(19) MacFarlane, D. R.; Sun, J.; Golding, J.; Meakin, P.; Forsyth, M. High Conductivity Molten Salts Based on the Imide Ion. *Electrochim. Acta* **2000**, *45*, 1271–1278.

(20) Kühnel, R.-S. S.; Lübke, M.; Winter, M.; Passerini, S.; Balducci, A. Suppression of Aluminum Current Collector Corrosion in Ionic Liquid Containing Electrolytes. *J. Power Sources* **2012**, *214*, 178–184.

(21) Balducci, A.; Dugas, R.; Taberna, P. L. P. L.; Simon, P.; Plée, D.; Mastragostino, M.; Passerini, S. High Temperature Carbon–carbon Supercapacitor Using Ionic Liquid as Electrolyte. *J. Power Sources* **2007**, *165*, 922–927.

(22) Arbizzani, C.; Biso, M.; Cericola, D.; Lazzari, M.; Soavi, F.; Mastragostino, M. Safe, High-Energy Supercapacitors Based on Solvent-Free Ionic Liquid Electrolytes. *J. Power Sources* **2008**, *185*, 1575–1579.

(23) Lazzari, M.; Soavi, F.; Mastragostino, M. Mesoporous Carbon Design for Ionic Liquid-Based, Double-Layer Supercapacitors. *Fuel Cells* **2010**, *10*, 840–847.

(24) Sillars, F. B.; Fletcher, S. I.; Mirzaeian, M.; Hall, P. J. Variation of Electrochemical Capacitor Performance with Room Temperature Ionic Liquid Electrolyte Viscosity and Ion Size. *Phys. Chem. Chem. Phys.* **2012**, *14*, 6094–6100.

(25) Matsumoto, H.; Matsuda, T.; Miyazaki, Y. Room Temperature Molten Salts Based on Trialkylsulfonium Cations and Bis(trifluoromethylsulfonyl)imide. *Chem. Lett.* **2000**, 1430–1431.

(26) Fang, S.; Yang, L.; Wei, C.; Peng, C.; Tachibana, K.; Kamijima, K. Low-Viscosity and Low-Melting Point Asymmetric Trialkylsulfonium Based Ionic Liquids as Potential Electrolytes. *Electrochem. Commun.* **2007**, *9*, 2696–2702.

(27) Wei, D.; Ng, T. W. Application of Novel Room Temperature Ionic Liquids in Flexible Supercapacitors. *Electrochem. Commun.* **2009**, *11*, 1996–1999.

(28) Orita, A.; Kamijima, K.; Yoshida, M.; Yang, L. Application of Sulfonium-, Thiophenium-, and Thioxonium-Based Salts as Electric Double-Layer Capacitor Electrolytes. *J. Power Sources* **2010**, *195*, 6970–6976.

(29) Noofeli, A.; Hall, P. J.; Rennie, A. J. R. Ionic Liquid Based EDLCs: Influence of Carbon Porosity on Electrochemical Performance. *Faraday Discuss.* **2014**, *FD 172*, 163–177.

(30) Anouti, M.; Timperman, L.; el hilali, M.; Boisset, A.; Galiano, H. Sulfonium Bis(trifluorosulfonimide) Plastic Crystal Ionic Liquid as an Electrolyte at Elevated Temperature for High-Energy Supercapacitors . *J. Phys. Chem. C* **2012**, *116*, 9412–9418.

(31) Krause, A.; Balducci, A. High Voltage Electrochemical Double Layer Capacitor Containing Mixtures of Ionic Liquids and Organic Carbonate as Electrolytes. *Electrochem. Commun.* **2011**, *13*, 814–817.

(32) Brandt, A.; Ramirez-Castro, C.; Anouti, M.; Balducci, A. An Investigation about the Use of Mixtures of Sulfonium-Based Ionic Liquids and Propylene Carbonate as Electrolytes for Supercapacitors. *J. Mater. Chem. A* **2013**, *1*, 12669–12678.

(33) Coadou, E.; Timperman, L.; Jacquemin, J.; Galiano, H.; Hardacre, C.; Anouti, M. Comparative Study on Performances of Trimethyl-Sulfonium and Trimethyl-Ammonium Based Ionic Liquids in Molecular Solvents as Electrolyte for Electrochemical Double Layer Capacitors. *J. Phys. Chem. C* **2013**, *117*, 10315–10325.

(34) Baokou, X.; Anouti, M. Physical Properties of a New Deep Eutectic Solvent Based on a Sulfonium Ionic Liquid as a Suitable Electrolyte for Electric Double-Layer Capacitors. *J. Phys. Chem. C* **2015**, *119*, 970–979.

(35) Pohlmann, S.; Olyschläger, T.; Goodrich, P.; Alvarez Vicente, J.; Jacquemin, J.; Balducci, A. Azepanium-Based Ionic Liquids as Green Electrolytes for High Voltage Supercapacitors. *J. Power Sources* **2015**, *273*, 931–936.

(36) Bhattacharjee, A.; Luís, A.; Santos, J. H.; Lopes-da-Silva, J. A.; Freire, M. G.; Carvalho, P. J.; Coutinho, J. A. P. Thermophysical Properties of Sulfonium- and Ammonium-Based Ionic Liquids. *Fluid Phase Equilib.* **2014**, *381*, 36–45.

(37) Lee, C.-P.; Peng, J.-D.; Velayutham, D.; Chang, J.; Chen, P.-W.; Suryanarayanan, V.; Ho, K.-C. Trialkylsulfonium and Tetraalkylammonium Cations-Based Ionic Liquid Electrolytes for Quasi-Solid-State Dye-Sensitized Solar Cells. *Electrochim. Acta* **2013**, *114*, 303–308.

(38) Machanová, K.; Boisset, A.; Sedláková, Z.; Anouti, M.; Bendová, M.; Jacquemin, J. Thermophysical Properties of Ammonium-Based Bis[(trifluoromethyl)sulfonyl]imide Ionic Liquids: Volumetric and Transport Properties. *J. Chem. Eng. Data* **2012**, *57*, 2227–2235.

(39) Gardas, R. L.; Coutinho, J. A. P. Extension of the Ye and Shreeve Group Contribution Method for Density Estimation of Ionic Liquids in a Wide Range of Temperatures and Pressures. *Fluid Phase Equilib.* **2008**, *263*, 26–32.

(40) Ye, C.; Shreeve, J. M. Rapid and Accurate Estimation of Densities of Room-Temperature Ionic Liquids and Salts. *J. Phys. Chem. A* **2007**, *111*, 1456–1461.

(41) Angell, C. A. Liquid Fragility and the Glass Transition in Water and Aqueous Solutions. *Chem. Rev.* **2002**, *102*, 2627–2650.

(42) Ribeiro, M. C. C. Low-Frequency Raman Spectra and Fragility of Imidazolium Ionic Liquids. *J. Chem. Phys.* **2010**, *133*, 024503–1–024503–6.

(43) Xu, W.; Cooper, E. I.; Angell, C. A. Ionic Liquids: Ion Mobilities, Glass Temperatures, and Fragilities. *J. Phys. Chem. B* **2003**, *107*, 6170–6178.

(44) Xu, K.; Ding, S. P.; Richard Jow, T. Toward Reliable Values of Electrochemical Stability Limits for Electrolytes. *J. Electrochem. Soc.* **1999**, *146*, 4172–4178.

(45) MacFarlane, D. R.; Tachikawa, N.; Forsyth, M.; Pringle, J. M.; Howlett, P. C.; Elliott, G. D.; Davis, J. H.; Watanabe, M.; Simon, P.; Angell, C. A. Energy Applications of Ionic Liquids. *Energy Environ. Sci.* **2014**, *7*, 232–250.

(46) Mastragostino, M.; Soavi, F. Strategies for High-Performance Supercapacitors for HEV. *J. Power Sources* **2007**, *174*, 89–93.

(47) Chmiola, J.; Yushin, G.; Gogotsi, Y.; Portet, C.; Simon, P.; Taberna, P. L. Anomalous Increase in Carbon Capacitance at Pore Sizes Less than 1 Nanometer. *Science* **2006**, *313*, 1760–1763.

(48) Huang, J.; Sumpter, B. G.; Meunier, V. A Universal Model for Nanoporous Carbon Supercapacitors Applicable to Diverse Pore Regimes, Carbon Materials, and Electrolytes. *Chem. - A Eur. J.* **2008**, *14*, 6614–6626.

(49) Merlet, C.; Rotenberg, B.; Madden, P. A.; Taberna, P.-L.; Simon, P.; Gogotsi, Y.; Salanne, M. On the Molecular Origin of Supercapacitance in Nanoporous Carbon Electrodes. *Nat. Mater.* **2012**, *11*, 306–10.

(50) Song, H.-K.; Jung, Y.-H.; Lee, K.-H.; Dao, L. H. Electrochemical Impedance Spectroscopy of Porous Electrodes: The Effect of Pore Size Distribution. *Electrochim. Acta* **1999**, *44*, 3513–3519.

(51) Jurczakowski, R.; Hitz, C.; Lasia, A. Impedance of Porous Au Based Electrodes. *J. Electroanal. Chem.* **2004**, *572*, 355–366.

(52) Pajkossy, T. Impedance Spectroscopy at Interfaces of Metals and Aqueous Solutions — Surface Roughness, CPE and Related Issues. *Solid State Ionics* **2005**, *176*, 1997–2003.

(53) Wang, G.; Zhang, L.; Zhang, J. A Review of Electrode Materials for Electrochemical Supercapacitors. *Chem. Soc. Rev.* **2012**, *41*, 797–828.

Table of Contents Graphic